Journal of Applied Geophysics 84 (2012) 14–28

Contents lists available at SciVerse ScienceDirect

Journal of Applied Geophysics

journal homepage: www.elsevier.com/locate/jappgeo

Time-lapse analysis of sparse 3D seismic data from the CO_2 storage pilot site at Ketzin, Germany

Monika Ivandic [a,*], Can Yang [a], Stefan Lüth [b], Calin Cosma [c], Christopher Juhlin [a]

[a] Department of Earth Sciences, Uppsala University, Villavägen 16, Uppsala 75236, Sweden
[b] Helmholtz-Zentrum Potsdam Deutsches GeoForschungsZentrum (GFZ), Telegrafenberg, 14473, Potsdam, Germany
[c] Vibrometric Oy, Taipaleentie 127, 01860 Perttula, Finland

ARTICLE INFO

Article history:
Received 29 October 2011
Accepted 17 May 2012
Available online 28 May 2012

Keywords:
CO_2 storage
Monitoring
Seismic acquisition
Time-lapse

ABSTRACT

The Ketzin pilot site is the first European on-shore CO_2 storage project site. Injection started in June 2008 and until the latest repeat survey in February 2011 around 45,000 t of CO_2 had been injected into a saline aquifer at approximately 630 m depth. Seismic monitoring methods that have been applied at the Ketzin site comprise baseline and repeat observations at various scales. We present here time-lapse results from sparse 3D seismic data measurements at Ketzin, which were acquired to link downhole surveys with conventional 3D surface seismic surveys. The results are consistent with the 3D seismic time-lapse studies over the injection site and show that the sparse 3D geometry can be used to map the CO_2 in the reservoir at a significantly lower effort than the conventional 3D surveying. The last repeat survey indicates preferential migration of the CO_2 to the west. There are no indications of migration into the caprock on either of the repeat surveys.

1. Introduction

One of the technological options for reducing net CO_2 emissions to the atmosphere includes capture and geological storage of CO_2. In April 2004, the CO_2SINK project started as the first onshore CO_2 storage test in Europe with a focus on a better understanding of geological CO_2 storage operations in a saline aquifer. The research site is located at Ketzin, ~15 km northwest of Potsdam, Germany (Fig. 1) and the target saline aquifer of the Triassic Stuttgart Formation is at a depth of around 630–650 m at the site. Three boreholes were drilled, one injection well (Ktzi 201) and two observation wells (Ktzi 200 and Ktzi 202), each to a depth of about 800 m (Prevedel et al., 2008). CO_2 injection started on the 30th of June 2008. Different seismic methods, such as time-lapse Vertical Seismic Profiling (VSP), Crosswell, Moving Source Profiling (MSP) and surface seismics have been employed to detect and monitor the reservoir. During the Fall of 2005 a 3D reflection seismic surveying was acquired. The main objectives of the first 3D survey were to determine the structural geometry for flow pathways within the reservoir, to provide a baseline for comparison before and after injection and, finally, to provide detailed subsurface images near the injection borehole for the drilling operations (Juhlin et al., 2007).

A critical factor in time-lapse seismic monitoring is the repetition of the seismic experiment between two or more surveys as accurately as possible. The method involves acquisition, processing and interpretation of repeated seismic surveys over a production/injection site with the aim of understanding the changes in the reservoir over time. Time-lapse seismic imaging has been shown to be an effective monitoring tool for CO_2 injected into a saline aquifer (Arts et al., 2004; Brevik et al., 2000; Eiken et al., 2000). The Sleipner offshore CO_2 storage project in Norway is an excellent demonstration of the successful application of time-lapse surface seismic methods to CO_2 plume monitoring (Chadwick et al., 2010).

At Ketzin the first 3D surface seismic repeat survey was conducted in Autumn 2009 over a limited area, and therefore is referred to as the "mini-3D". Time-lapse processing of the baseline and repeat 3D data set imaged a CO_2 induced change of reflection amplitude centered at the injection well (Bergmann et al., 2010; Ivanova et al., 2012).

During the 3D campaign seven 2D lines in a "star" configuration, i.e. with a radial distribution of acquisition profiles directed toward the approximate location of the injection well (Fig. 1), were also acquired in order to link downhole surveys with 3D surface seismic surveys. As the vertical seismic profiling (VSP) and moving source profiling (MSP) utilize a VIBSIST source, it was considered advantageous to acquire surface seismic data in the vicinity of the injection site with the same source (Juhlin et al., 2006). The initial objectives of the "star" surveys were to identify changes in the seismic response related to the injection of CO_2 and to monitor the migration of CO_2 in the reservoir along these 2D lines. However, with all the lines simultaneously active during the acquisition, it was also possible to generate a sparse 3D cube and, thus, to compare it with the one from the regular 3D seismic data. The baseline survey was acquired in 2005 along with the regular 3D survey. Up to the time of the 1st repeat survey in September 2009 a relatively small amount of CO_2 had been

* Corresponding author. Tel.: +46 18 4717157; fax: +46 18 4712592.
E-mail address: monika.ivandic@geo.uu.se (M. Ivandic).

0926-9851/$ – see front matter © 2012 Elsevier B.V. All rights reserved.
doi:10.1016/j.jappgeo.2012.05.010

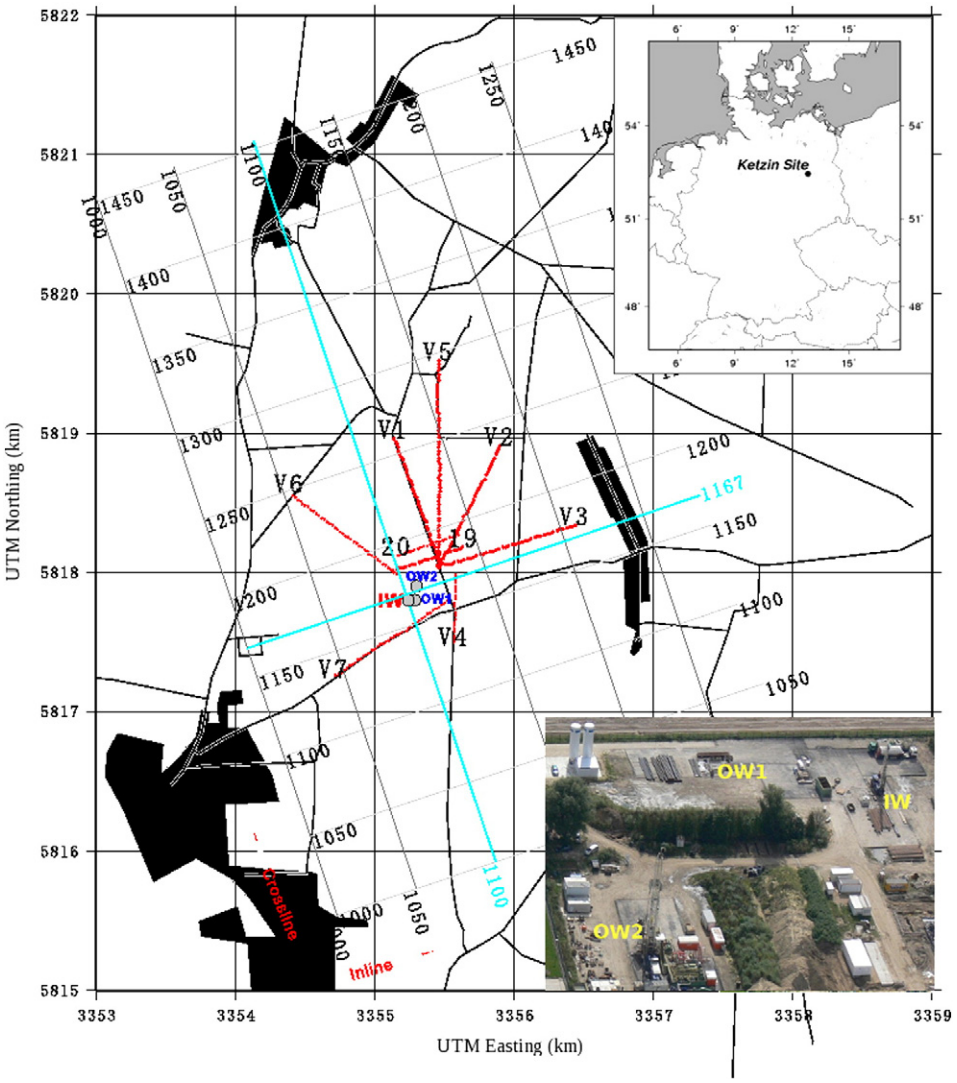

Fig. 1. Location of the Ketzin site in Germany is at the upper right corner. Sparse 3D and full 3D seismic survey area with the system of inlines and crosslines, the location of the CO_2 injection well (IW) and two observation wells (OW1, OW2). The sparse 3D survey lines (V1 to V7) and two short receiver lines (19 and 20) are marked by red dashed lines. Detailed figure with the three wells is shown at the bottom right corner. One inline 1167 and one crossline 1100, marked in blue, will be displayed later.

injected (22–25 kt) and by the time of the 2nd repeat survey in February 2011 about 45 kt had been injected. Processing of the "star" data has focused on generating sparse 3D volumes that can be compared with results from the mini-3D survey (Ivanova et al., 2012). For comparison, the grid of inlines and crosslines were numbered as for the regular 3D surface seismic data. This simplified the cross-equalization of the time-lapse datasets and the results could be directly analyzed and compared with those from the regular 3D seismic survey. In this paper we present results from the sparse 3D surveys and comparisons with the regular 3D data and discuss the advantages and disadvantages of both acquisition geometries.

2. Geological setting and reservoir characterization

Fig. 2 shows the simplified geological structure of the site based on data obtained in the up to 800 m deep CO_2SINK boreholes. The target reservoir, the Stuttgart Formation, is on average 80 m thick and contains lithologically heterogeneous sandy channel-facies rocks of good reservoir properties alternating with muddy, flood-plain facies rocks of poor reservoir quality. The Weser and Arnstadt formations form an approximately 210 m thick caprock section above the Stuttgart Formation and consist mainly of claystone, silty claystone, and anhydrite (Förster et al., 2006). At the top of the Weser formation is a 10–20 m thick anhydrite layer known as the Heldburg-Gips. The layer gives a strong reflection and is called the K2 (Keuper) reflector. Above the CO_2 reservoir caprock, at a depth of about 250 to 400 m, is another major pre-Tertiary reservoir. It consists of sandstone from the Jurassic period and was formerly used as storage for city gas and natural gas.

3. Data acquisition

The mini-3D survey followed the same geometry as in the baseline, but with only 20 templates located in the vicinity of the injection site. The geophones and acquisition unit used in the 3D and sparse 3D surveys were the same. Acquisition lasted from the 25th of September through the 6th of November. About 3250 source points were activated using an accelerated EWGIII weight drop source during 34 days of active acquisition. The processing work flow for the mini-3D was the

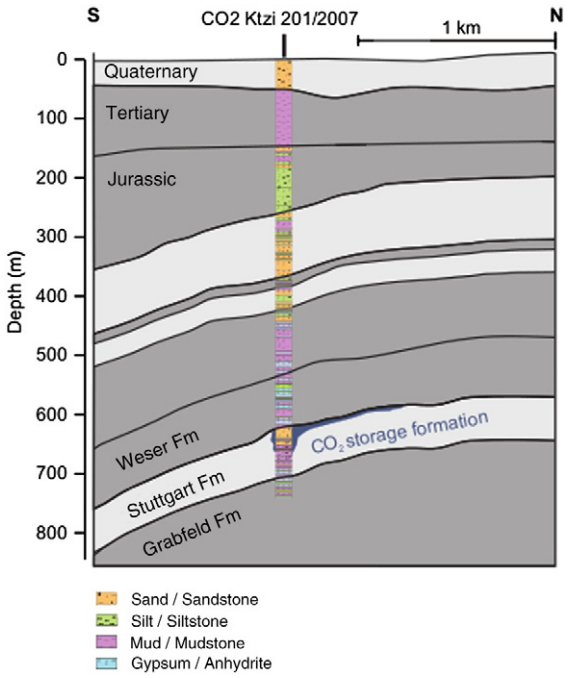

Fig. 2. Simplified geological structure of the site (after Förster et al. (2006)) with lithology of the injection well CO_2 Ktzi 201/2007.

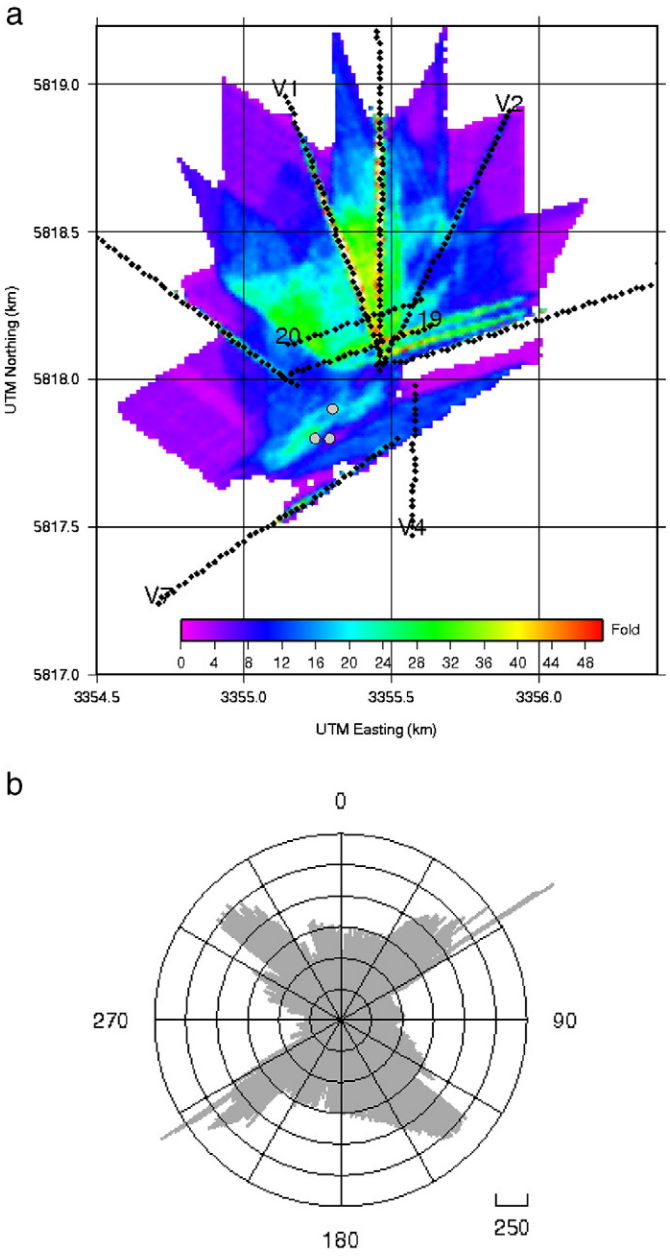

Fig. 3. a) Actual fold for the sparse 3D survey; b) source–receiver azimuthal distribution for the boreholes area (inlines 1140–1200, crosslines 1075–1125).

same as the one used for the baseline 3D data with minor modifications related to changes in the refraction statics and the choice of bandpass filters. Details of the 3D baseline acquisition and processing are described in Juhlin et al. (2007) and of the repeat 3D processing in Ivanova et al.(2012).

Due to the infrastructure near the wells, the fold of the 3D surface seismic data over the injection site was as low as 10 for some CDP bins (Juhlin et al., 2007). Therefore, seven surface seismic shot/receiver lines (lines V1 to V7) and two shorter receiver lines (lines 19 and 20) near the injection site were designed to obtain better images near this area. Lines were chosen to be directed toward the approximate location of the injection well, resulting in a star-like geometry (Fig. 1). Source points were activated along the lines V1 to V7, and data were recorded simultaneously on all the lines, giving a standard 2D survey for each line and a focused sparse 3D survey near the wells.

A consequence of an irregular geometry is an uneven fold and azimuth distribution. Actual fold for the sparse 3D survey is also variable with high values along the 2D lines. Relatively high fold values, around 20–25, characterize also the area around the injection site (Fig. 3a). However, the highest fold is directly north of the injection site since it was expected that the CO_2 would most likely migrate toward the top of the anticline. Source–receiver azimuthal distribution for the area around the boreholes reveals a similar pattern with fairly large variations in offsets >500 m (Fig. 3b).

The 1st "star" repeat survey was, like the baseline, carried out in close temporal succession to the respective 3D survey. The baseline sparse 3D survey was acquired with a VIBSIST-1000 source (Yordkayhun et al., 2009), whereas in the repeat surveys another type, but similar, source was used, the VIBSIST-3000. The VIBSIST is a swept impact seismic source (Park et al., 1996) which combines the Vibroseis swept-frequency and the Mini-Sosie (Barbier et al., 1976) multi-impact techniques. Impulsive impacts are generated in a sequence with increasing impact frequency, with up to several hundred pulses. A shift and stack method (Park et al., 1996) is then applied to the raw data to generate seismograms for conventional reflection seismic processing.

The first repeat survey was acquired in 5 days in September 2009. The same acquisition system was used as in the baseline survey (Bergmann et al., 2011). In February 2011, the second repeat survey was acquired, and all the equipment and parameters were the same as in the 2009 and baseline surveys, except that the recording system was updated to a SERCEL 428XL. The survey was acquired within 8 days. Because of weather conditions and permission issues, some shots were skipped. The detailed parameters are shown in Table 1. The spacing between shots was 12 m and between receivers was 24 m in all three surveys. Sources were placed 6 m before and 6 m behind the respective receivers. Data recording was conducted with single 28 Hz geophones, planted in 0.2 m deep holes.

4. Data processing

Processing steps were somewhat modified from the 3D surface seismic data processing work flow (Juhlin et al., 2007) and kept relatively

Table 1
Acquisition parameters for the sparse 3D seismic surveys.

Parameter	Value		
Year	Baseline 2005	1st repeat 2009	2nd repeat 2011
Month	November	September	February
Source point spacing	12 m		
Receiver point	24 m		
Number of shot points (7 lines)	V1–81 V2–81 V3–82 V4–28 V5–124 V6–81 V7–79	V1–84 V2–83 V3–82 V4–16 V5–121 V6–82 V7–83	V1–84 V2–84 V3–88 V4–14 V5–120 V6–84 V7–72
Geophones	28 Hz single		
Sampling	1 ms		
Recording length	30 s		
Source	VIBSIST-1000	VIBSIST-3000	VIBSIST-3000

simple in order to avoid the risk of introducing artifacts. Processing was performed using the Globe Claritas software. Since the data sets had to be time-lapse analyzed, nearly the same processing parameters were applied to each data set, except for refraction and residual statics, as the surveys were carried out during different weather and ground conditions. Initial processing consisted of decoding the sweeps for each shot and then stacking them to generate conventional shot gathers (Cosma and Enescu, 2001). In order to increase repeatability in fold and azimuthal coverages, traces which were not present in either the baseline or repeat data sets were excluded from further processing. The next step included geometry assignment and trace editing. The geometry was extracted from the headers and the data were binned to match with the 3D surface data. The grid of inlines and crosslines were numbered as for the 3D surface seismic data. The injection borehole is located approximately where inline 1165 and crossline 1100 intersect (Fig. 1). After this step, the decoded shots from the three surveys were compared to check the repeatability. Fig. 4 shows an example from line1, shot1. A comparison of the amplitude spectra of the baseline and both repeat surveys, shown in Fig. 5, reveals that the energy content at higher frequencies is lower in the repeat surveys in comparison to the baseline. This is probably due to the different source type used in the repeat surveys (modified by mounting it on a construction vehicle, which allowed better mobility and higher production rate) and near-surface

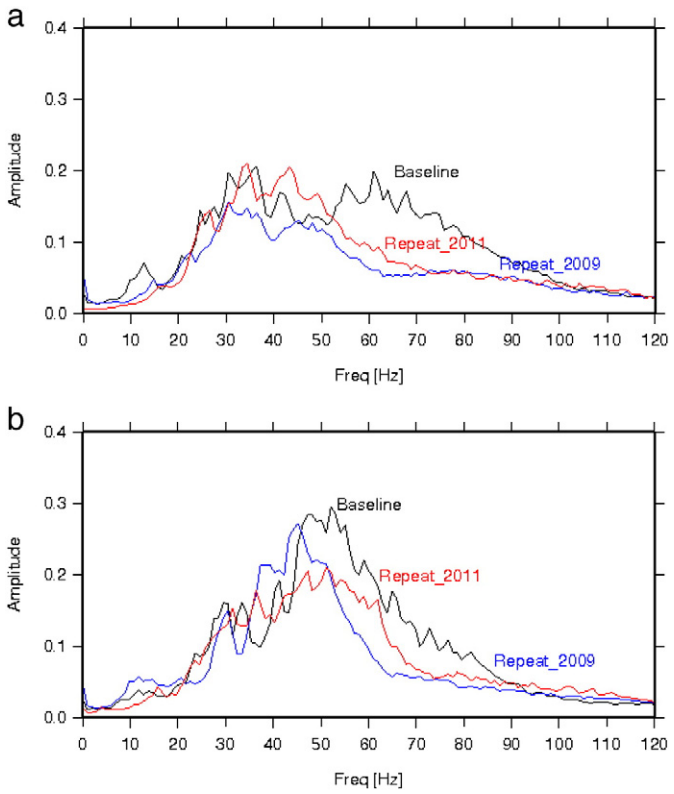

Fig. 5. a) Amplitude spectra from one selected shot from line V2 for baseline, 1st repeat and 2nd repeat and b) same as a) for a selected shot from line V7.

conditions. These differences in spectral content were reduced after the application of spectral equalization, and further cross-equalization, i.e. the application of shaping filtering (Robinson and Treitel, 1980), minimized any residual differences between the surveys.

Refraction statics were calculated separately for the different data sets, because of the near-surface/water table variations. The quality of the first break picks is variable, but in general better for larger offsets.

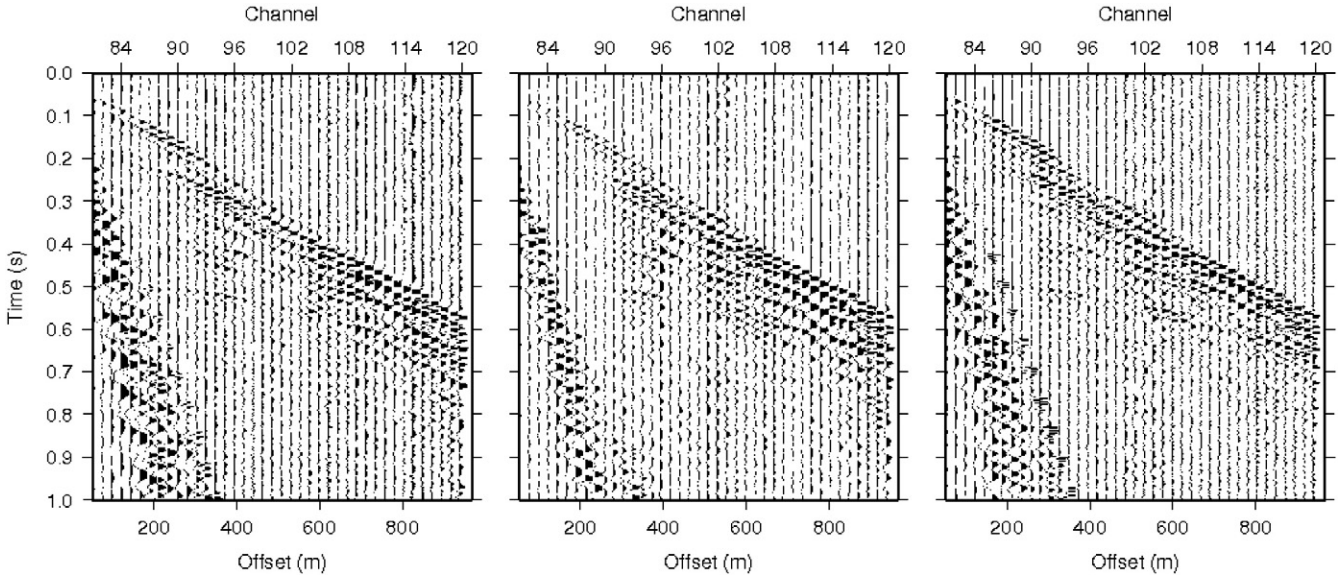

Fig. 4. Example of three raw shot gathers from the same source point, a) baseline survey, b) 1st repeat and c) 2nd repeat surveys.

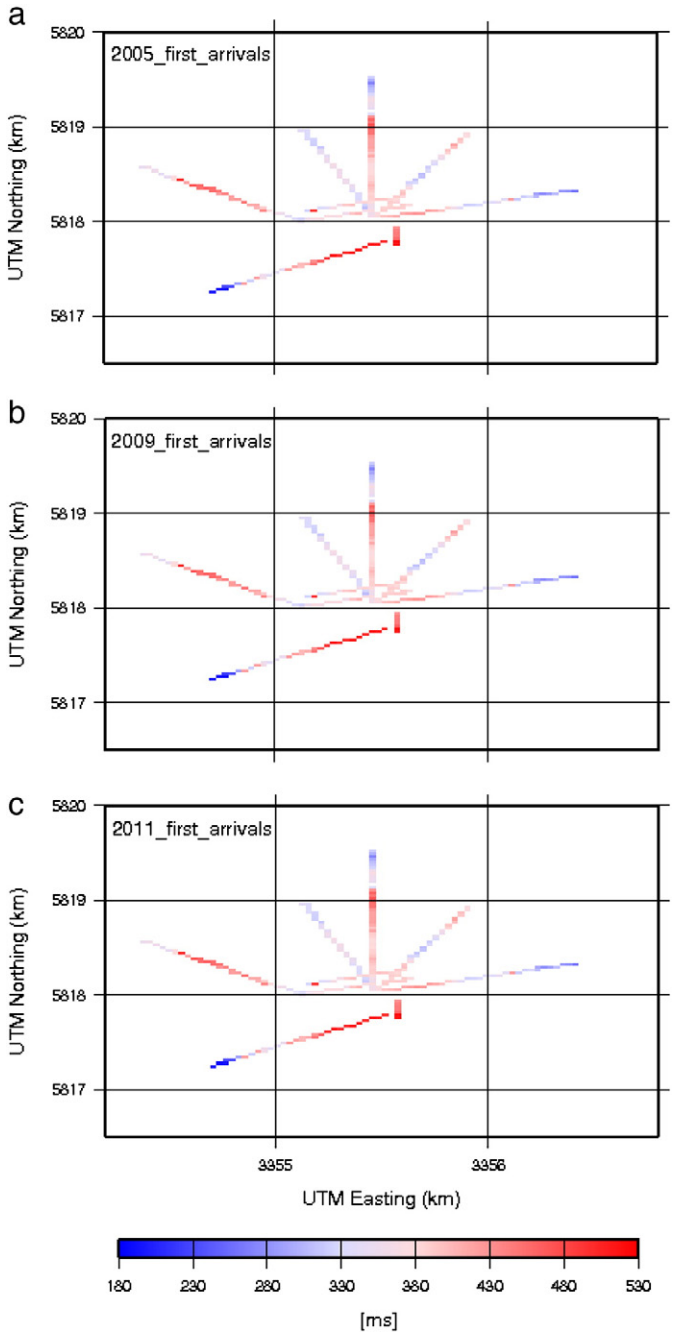

Fig. 6. Comparison of first arrivals between baseline and repeat surveys for the receiver gathers: averaged first arrivals for the a) baseline survey, b) 1st repeat and c) 2nd repeat surveys.

However, the data from 2009 are more noisy, thus they are more difficult to accurately pick than the other two data sets. Furthermore, in all three data sets, the lowest S/N ratios are found along line V7, which is located along the main road to Ketzin. Near offset traces also showed significant effects from ground roll, so first arrivals were picked in a 200–500 m offset window. As new coordinates of the source and receiver locations were re-surveyed for the repeat measurements, they were checked for consistency (Fig. 6). A two layer model from the 3D seismic data processing (Juhlin et al., 2007) with a velocity of 1000 m/s for the 13–16 meter thick upper layer and 1800 m/s for the lower one was used as a starting model for the calculation of the refraction statics.

After application of the refraction statics and later residual statics the coherency of the shot and receiver gathers were improved. Surface consistent deconvolution was carried out on both shot and receiver gathers, as well as bandpass filtering and air wave removal. Fig. 7 shows the shot gathers, shown previously in Fig. 4, after processing, but before the NMO correction. Later, NMO corrections, stacking and FX-deconvolution were applied on the data sets. The final stacked images were not migrated due to the uneven fold distribution. An attempt to apply migration to the sparse 3D data resulted in severe artifacts which appeared as broad circular arcs, confirming expected negative effects of the irregular acquisition geometry (e.g., Canning and Gardner, 1998; Qin et al., 2005; Tang, 2007). An overview of the processing steps is given in Table 2.

All data were processed in a consistent manner from prestack to poststack, but certain differences in phase, amplitudes and time shifts still existed. The aim of cross-equalization is to remove processing and acquisition differences between time-lapse seismic surveys, so comparison between them can be interpreted in terms of actual fluid related changes.

Cross-equalization requires a wavelet operator, estimated in a time window, to shape and match data from the monitor survey to the baseline survey. The filter can contain up to four basic elements: time corrections, RMS energy balancing, frequency bandwidth normalization, and phase matching (Ross et al., 1996). The Pro4D program from Hampson-Russell Ltd. was used for the time-lapse analysis.

The baseline data set is set as a reference volume and does not change during the entire processing. The repeat data sets are updated after every processing step. In the Pro4D program the correlation procedure is defined by its window length and the start time of the correlation. The very shallow parts of the data sets were excluded from the calibration window because of poor subsurface coverage due to the dominance of large offsets.

The first step was phase and time shifting. A design window above the reservoir was chosen and a trace-by-trace processing mode was used. The estimated phase and time shifts were then applied to the monitor data. The next step was the application of the shaping filter, which is used to estimate a transfer function that matches the frequency content, phase, time, and average power of the two data sets using a Wiener–Levinson time-domain approach (Rickett and Lumley, 2001). The same time-window above the reservoir was used. Here, however, the global average processing mode was found to give the best results.

The next calibration steps were the application of the cross-correlation statics and time variant shifts. They were performed on the data sets in order to correct for the near-surface effects, as well as to correct for the production induced time-delays below the reservoir. Finally, the cross-normalization process was applied to the monitor data to ensure that the root-mean-square (RMS) amplitudes of common traces are similar. In principle, the seismic difference images after this processing then represent reservoir property changes.

5. Time-lapse results

By comparing the baseline with the two repeat data sets potential changes related to CO_2 injection can be detected. Figs. 8 and 9 show final stacked sections for the baseline and the two repeat data sets. Presented are the inlines and crosslines in the vicinity of the injection borehole, where the time-lapse effects are expected to be most prominent. The area around the target reservoir is marked with a green rectangle (top at 480 ms, bottom at 560 ms). Changes in amplitudes are found within the Stuttgart Formation at approximately 530 ms near the injection borehole in both the inline and crossline directions. The observed stronger reflections in the target area are interpreted as due to injected CO_2. The presence of CO_2 should enhance the impedance contrast of the internal layers in the aquifer (Kazemeini et al., 2010).

Although the parameters of the seismic acquisition and processing steps are almost the same, there are some differences among the stacked

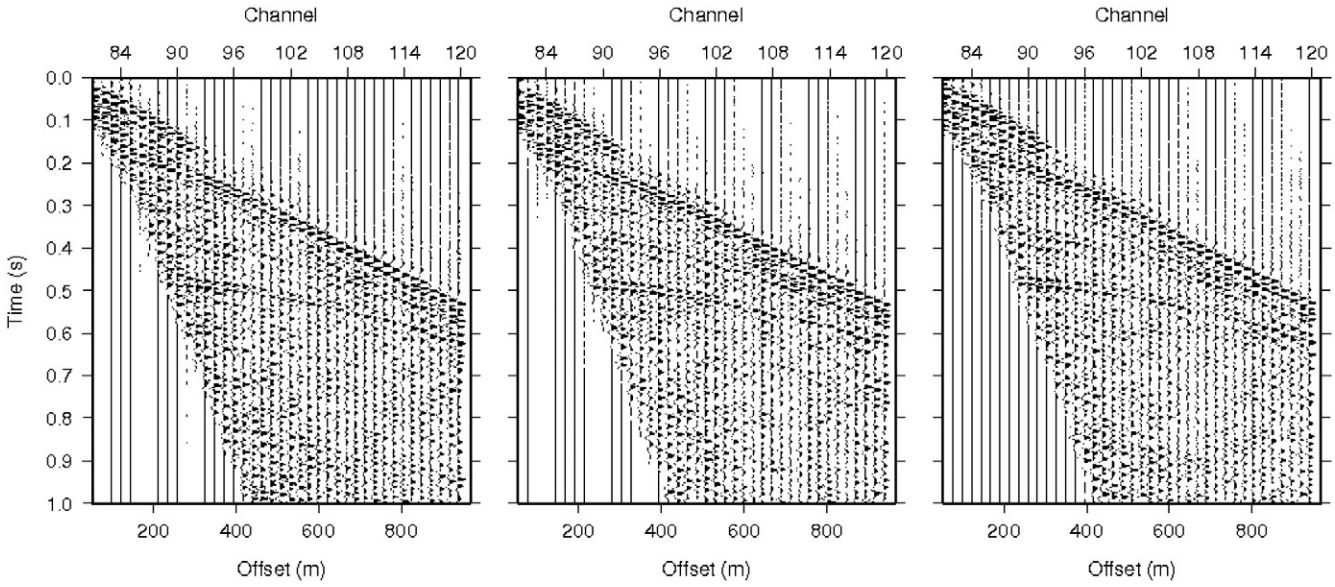

Fig. 7. Same as Fig. 4, after processing applied up to step 15 in Table 2.

seismic data sets. Comparison of the maximum cross-correlation coefficients and correlation time-shifts above the reservoir layer before (Fig. 10) and after time-lapse analysis (Fig. 11) reveals a significant improvement in seismic matching for both repeat surveys. Another parameter used to assess the quality of the seismic match is the normalized RMS error (NRMS) between the volumes. The NRMS error measures the level of amplitude in the difference trace normalized by the average of the base and monitor traces. A perfect match gives a value of 0. Fig. 12 shows maps for the cross-calibrated seismic sub-volumes in the time-interval 100–700 ms for both repeat surveys. The NRMS outside of the injection area is between 0.35 and 0.55 and the general distribution is roughly consistent with the fold values (Fig. 3a), implying good repeatability in high fold areas despite some variations in data quality. The NRMS values of 0.15–0.25 estimated from the time-lapse processed mini-3D data indicate higher repeatability of those data for most of the survey area (Ivanova et al., 2012).

Since time-discrepancies are minimized, subtraction of the two data sets from one another results in a section where the amplitude differences are enhanced. Difference images for the time-lapse processing results for the 1st repeat data set are shown in Fig. 13a and for the 2nd repeat in Fig. 13b.

In the 1st repeat seismic cube the observed CO_2 induced amplitude anomaly extends for ~120 m in the inline direction (crosslines 1095–1105) and ~75 m in the crossline direction (inlines 1162–1168). The amplitude anomaly observed in the 2nd repeat seismic cube extends for some 290 m in the inline direction (cross-lines 1086–1111) and about 190 m in the crossline direction (inlines 1159–1172). In both data sets the anomaly is visible within a time window of less than 15 ms (525–538 ms). There are no time-lapse anomalies observed above the K2 reflection in the vicinity of the injection site, indicating that there is no CO_2 leakage from the reservoir level.

Table 2
Processing sequence applied to the sparse 3D datasets.

Step	Parameters		
	Baseline (2005)	1st repeat (2009)	2nd repeat (2011)
1	Read and decode SEGD data		
2	Create and apply geometry		
3	Edit bad traces and reverse traces polarity		
4	Pick first arrivals: offset range 200–500 m		
5	Removal 50 Hz (electricity line at some receiver locations)		
6	Geometrical spreading compensation		
7	Band-pass filter: Butterworth 7–14–120–200 Hz		
8	Surface consistent deconvolution: filter 120 ms, gap 16 ms, white noise 0.1%		
9	Ground roll mute		
10	Spectral equalization 20–40–90–120		
11	Time-variant band-pass filter 0–300 ms: 15–30–85–125 Hz 350–570 ms: 14–28–80–120 Hz 620–1000 ms: 12–25–70–105 Hz		
12	Refraction statics: datum 30 m, replacement velocity 1800 m/s, v0 1000 m/s		
13	Velocity analysis		
14	Residual statics		
15	NMO correction		
16	Stack		
17	FX-deconvolution		

6. Comparison with "regular" 3D results and discussion

The site includes some infrastructure in the vicinity of the borehole, such as equipment and buildings on the former gas distribution site, which in the 3D survey resulted in lower actual subsurface coverage in those areas. Therefore, an irregular 3D geometry, like the "star"-configuration, can be useful in obtaining better coverage near the injection site. Another advantage of the sparse 3D survey compared to the regular 3D is the substantially lower cost and less time needed for seismic acquisition and processing. Furthermore, the 'star' geometry utilizes to a higher degree existing roads and, therefore, minimizes damage to agricultural fields. However, the resulting uneven fold and azimuth distributions over the survey area may lead to obscured actual amplitude anomalies and, thus, to unreliable data interpretation. Moreover, the introduction of amplitude artifacts may occur and, thus, data processing steps and parameters should be carefully chosen. Such fold variations negatively affect the final stacked images. These effects

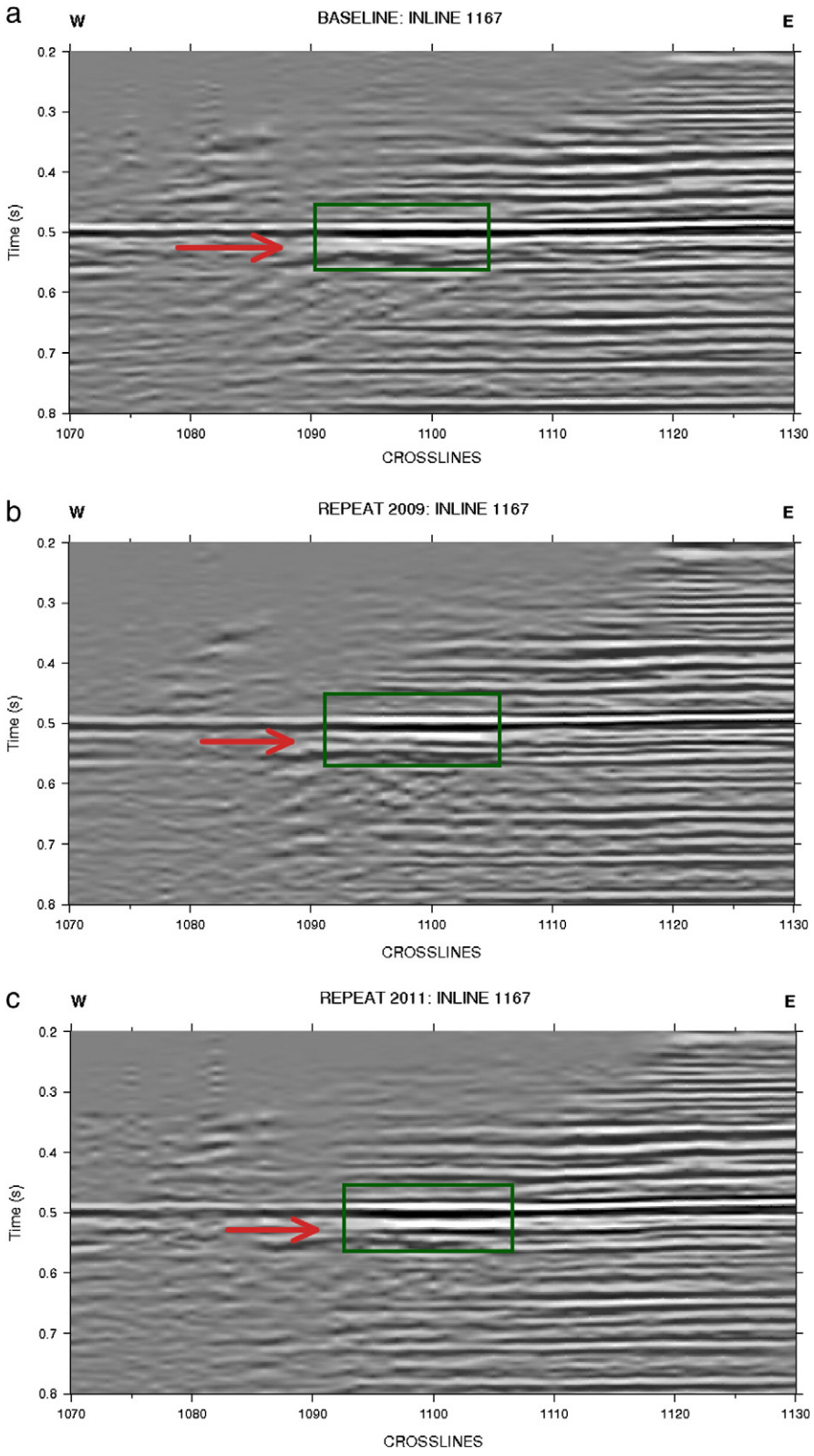

Fig. 8. Inline 1167 from the a) baseline, b) 1st repeat and c) 2nd repeat. The target and top seal layers are marked with a green rectangle, and the reservoir by red arrows. The location of the line is shown in Fig. 1.

could have potentially been reduced using, for instance, a flexible binning scheme (Schmelzbach et al., 2007; Yilmaz, 2001), but the same binning as in the mini-3D data set had to be used in order to align all the surveys onto a common grid.

Both the repeat sparse 3D and regular 3D surveys image the subsurface down to 1 s with local differences, mainly related to the reflection amplitudes, due to the fold variations between the two acquisition geometries (Fig. 14). The near Base Tertiary and Top Weser Formation

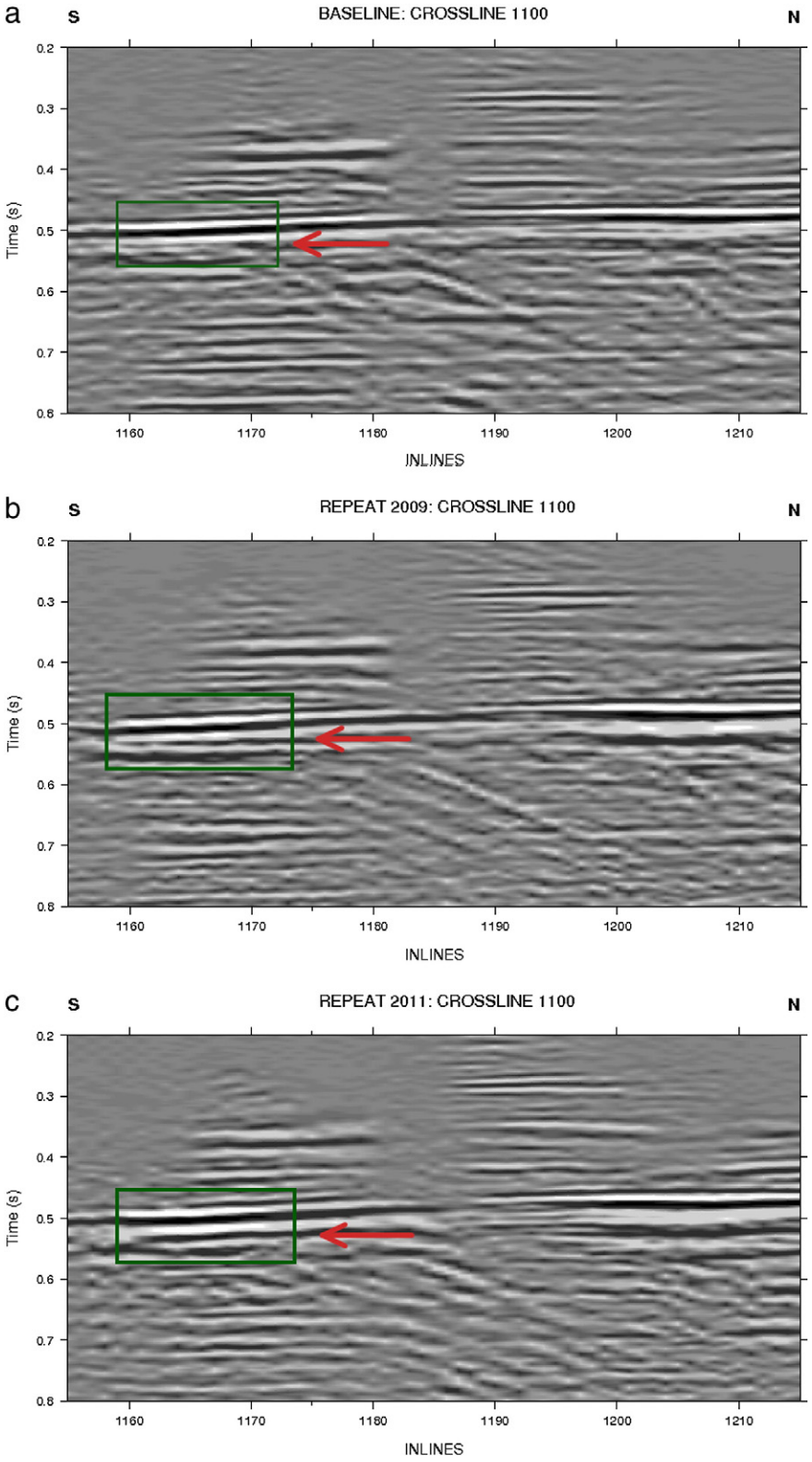

Fig. 9. Same as Fig. 8, but for crossline 1100.

(K2) are clearly identified in the stacks of both sparse and regular 3D data sets. Reflections from between the Base Tertiary and the K2 are generally less well constrained because of lower amplitudes, and could not even be mapped over the entire area with the sparse 3D data. However, the time-lapse analysis presented here shows that the time-lapse signature related to the CO_2 injection is observable in both sparse 3D

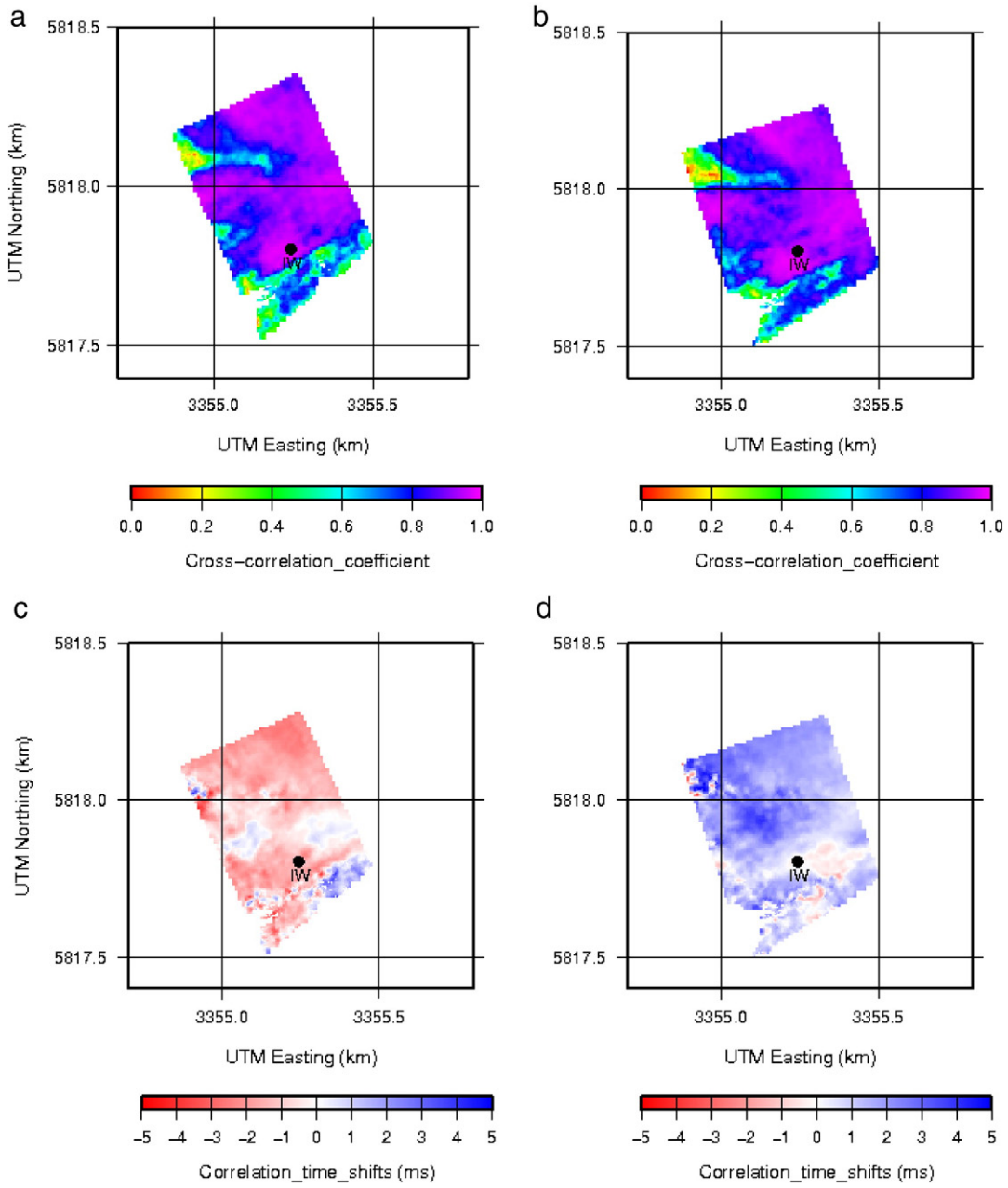

Fig. 10. a) and b) Maximum cross-correlation coefficients, and c) and d) correlation time-shifts above the reservoir before time-lapse analysis. a) and c) for the 1st repeat, and b) and d) for the 2nd repeat surveys.

repeat data sets, which is consistent with the time-lapse results of the mini-3D survey, which images a reflectivity increase centered around the injection well within the Stuttgart Formation.

Maps showing the distribution of the amplitude changes below the K2 horizon, i.e. migration pathways of CO_2 within the reservoir, for the sparse 3D data sets have been created in order to compare them with the amplitude difference map of the full fold 3D seismic data. Fig. 15a–c shows the amplitude difference horizons at the reservoir level for the cross-calibrated mini-3D, 1st and 2nd repeat data sets, respectively. A comparison of the results from the two repeat data sets from 2009 reveals that the CO_2 related anomaly observed in the sparse 3D data is of a reduced extent and significantly lower amplitude compared to the one observed in the mini-3D data. The CO_2 induced amplitude anomaly visible in the mini-3D data extends for some 350 m in the inline direction (crosslines 1085–1110), 250 m in the crossline direction (inlines 1155–1175) and 20 ms in time (515–535 ms) (Ivanova et al., 2012), i.e. over the about 3 times larger area than the one observed in the sparse 3D data set at the time of the 1st repeat survey in 2009. The most likely explanation for this discrepancy is the different acquisition geometry, i.e. the uneven fold distribution over the survey area. As mentioned above, unlike the 3D survey, here the reflections from between the Base Tertiary and the K2 could not be imaged over the entire area. Another parameter which might contribute to these differences is the accuracy of the refraction static corrections. Also, the 2009 sparse 3D data set appears to contain more noise, which affected the accuracy of the first arrival picking. As a consequence, direct mapping using the K2 as a calibration horizon did not produce useful results. Instead, in order to generate a useful map, it was necessary to cross-equalize the data, i.e. to correct variations in the seismic character not related to changes in the reservoir. This was not the case with either the mini-

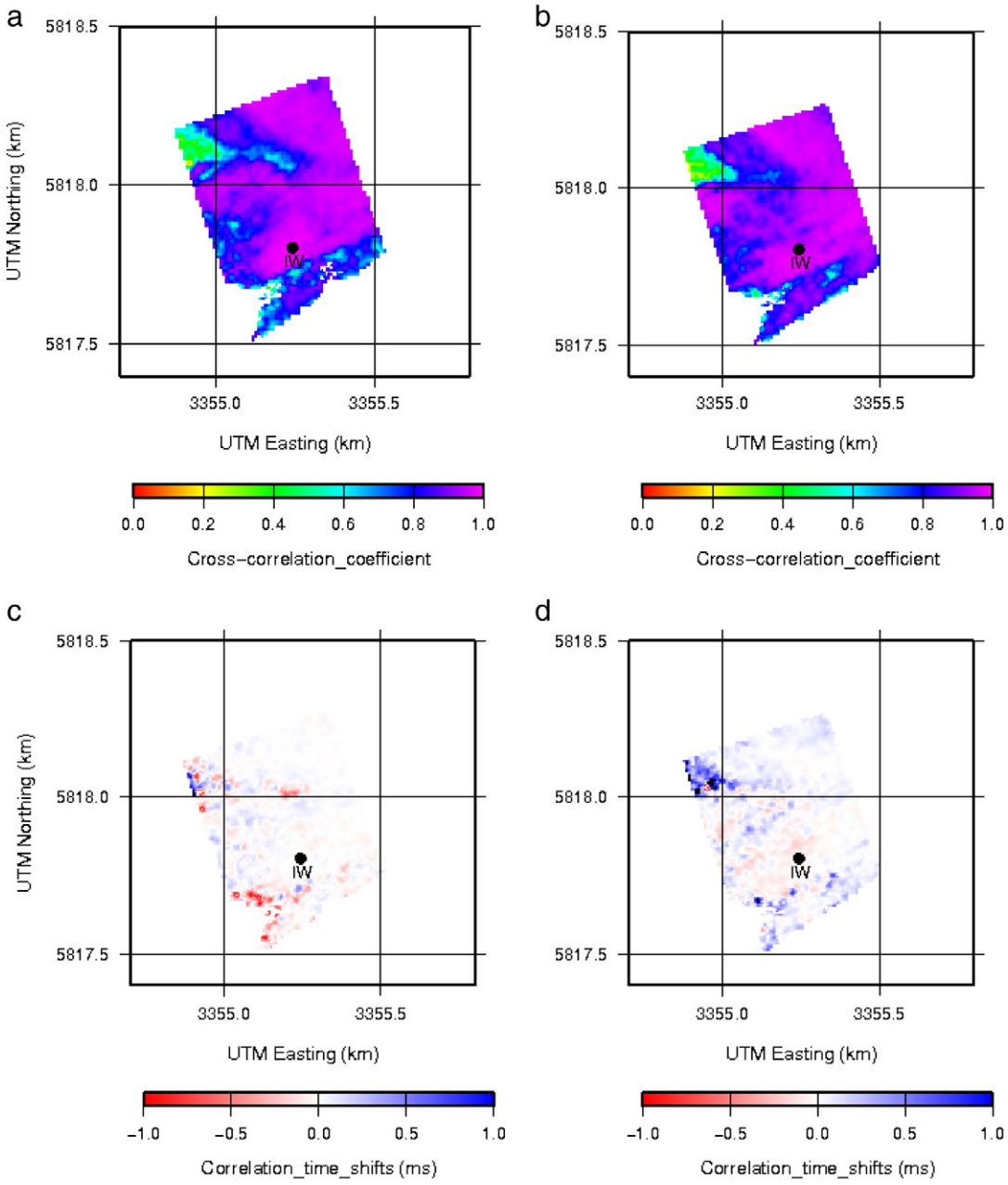

Fig. 11. a) and b) Maximum cross-correlation coefficients, and c) and d) correlation time-shifts above the reservoir after time-lapse analysis. a) and c) for the 1st repeat, and b) and d) for the 2nd repeat surveys.

3D or even with the 2nd sparse repeat data set. Despite the gentle dip in the area, Fig. 15d shows that the amplitude difference horizon at the reservoir level in the unmigrated data differs from the one in the migrated data set both in size and amplitude, implying that the migration process has a profound impact on the final image of the plume. Thus, the fact that the sparse 3D data were not migrated most likely considerably contributes to the differences in the images.

The anomaly observed in the 2011 repeat data is significantly stronger compared to the 1st repeat and shows high similarity in the vicinity of the injection borehole with the one from the mini-3D result. Here, however, the interpreted spreading of the anomaly is even more in the westerly direction, rather than toward the north. Consequently, the preferential movement to the west does not allow the "star" lines to be processed as 2D lines in order to track the anomaly. Moreover, previous time-lapse interpretation of the 2D data sets showed that at the time of the 1st repeat survey no CO_2 related time-lapse signature is observable where the 2D lines allow monitoring of the reservoir (Bergmann et al., 2011). The pronounced westward tendency present in the data sets from 2011 can be explained by the highly heterogeneous internal structure of the reservoir. Preliminary results from surface to downhole geoelectric surveys also indicate a more westerly migration of the CO_2 in the reservoir (Kiessling et al., 2010).

7. Conclusions

Uneven fold and higher noise levels in the sparse 3D seismic data do not allow a quantitative comparison, but can provide insight into how the injected CO_2 is spreading within the reservoir. The irregular 3D

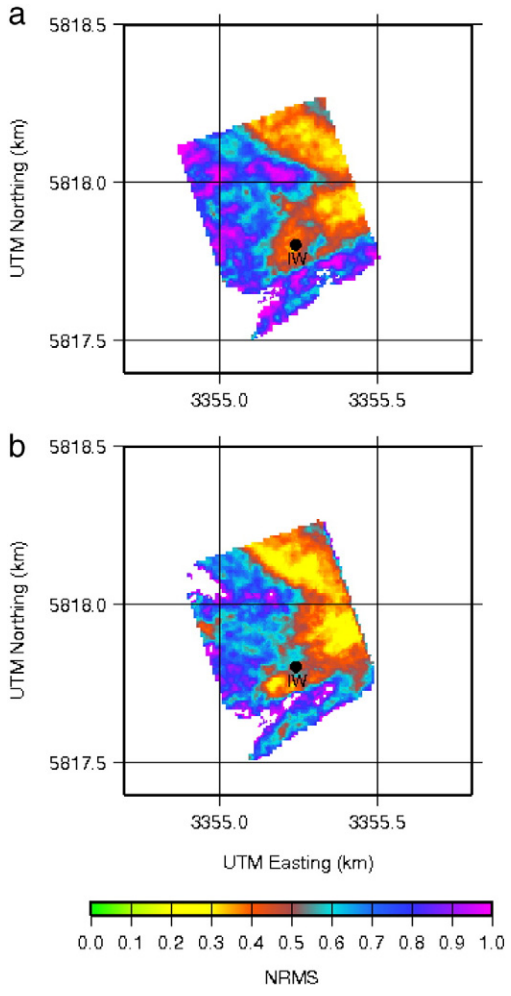

Fig. 12. NRMS error maps for the cross-calibrated seismic sub-volumes in the time-interval 100–700 ms for a) 1st repeat survey and b) 2nd repeat survey.

acquisition geometry provides a qualitative image of the amplitude changes due to the CO_2 injection in the vicinity of the borehole area.

The 2nd repeat sparse 3D survey reveals a significantly stronger anomaly compared to the 1st repeat and shows that the CO_2 plume appears to be moving preferentially toward the west. Although the sparse 3D results are not as detailed as in the true 3D time-lapse map and the apparent size of the anomaly is smaller, a similar migration pattern is observed in both data sets. The observed pattern is an indication of the heterogeneous permeability of the Stuttgart Formation, which strongly affects the plume geometry.

Significantly better results could potentially have been achieved with a more regular pattern of sources and receivers. An attempt to quantify the amount of CO_2 visible in the mini-3D seismic data resulted in somewhat lower quantity than the actual one injected at the time of the survey (Ivanova et al., 2012). implying that a "regular" network configuration could be a good approach for quantitative monitoring of CO_2 storage. Still, irregular acquisition, such as the "star" approach, should not be discarded in attempts to resolve the actual changes within the reservoir. As noted earlier, the location of the "star" lines was mainly controlled by the aim of improved subsurface coverage toward the top of the anticline, to which CO_2 was most likely expected to migrate (Juhlin et al., 2006). Due to the complex structure of the reservoir, with a preferential flow of CO_2 toward the west, the actual fold coverage did not serve well in achieving a better image of the anomaly. Improving the fold by simply introducing more lines in the area of interest can result in a low-cost and effective solution for mapping the migration of the CO_2 plume away from the injection site. Nevertheless, the results presented here are consistent with observations obtained from the mini-3D data and show that the "star" geometry can be successfully used to track the migration of the CO_2 plume within the Stuttgart Formation, as well as the potential migration into the caprock.

Acknowledgments

The 2005 baseline survey was mainly funded by the European Union (project CO_2SINK, no. 502599), the 2009 and 2011 repeat surveys were funded by the Geotechnologien Programme of the German Federal Ministry of Education and Research, BMBF (project 3DRep1, AZ 03G0679A). Globe Claritas™ under license from the Institute of Geological and Nuclear Sciences Limited, Lower Hutt, New Zealand was used to process the seismic data. Hampson and Russell (CGG Veritas) provided Pro4D for the time-lapse analysis. Can Yang would also like to thank the China Scholarship Council for providing him with a scholarship for his PhD study.

References

Arts, R., Eiken, O., Chadwick, A., Zwegel, P., van der Meer, B., Zinszner, B., 2004. Monitoring of CO_2 injection at Sleipner using time-lapse seismic data. Energy 29 (2004), 1383–1392.

Barbier, M.G., Bondon, P., Mellinger, R., Viallix, J.R., 1976. Mini-SOSIE for land seismology. Geophysics Prospecting 24, 518–527.

Bergmann, P., Giese, R., Götz, J., Ivanova, A., Juhlin, C., Juhojuntti, N., Kashubin, A., Lüth, S., Yang, C., Zhang, F., 2010. Preliminary results from 3D repeat seismics at the CO_2-SINK injection site, Ketzin, Germany. 72nd EAGE Conference & Exhibition incorporating SPE EUROPEC 2010, Barcelona, Spain, p. 201.

Bergmann, P., Yang, C., Luth, S., Juhlin, C., Cosma, C., 2011. Time-lapse processing of 2D seismic profiles with testing of static correction methods at the CO_2 injection site Ketzin (Germany). Journal of Applied Geophysics 75, 124–139.

Brevik, I., Eiken, O., Arts, R.J., Lindeberg, E., Causse, E., 2000. Expectations and results from seismic monitoring of CO_2 injection into a marine aquifer. 62nd EAGE Meeting, Glasgow, Paper B-21.

Canning, A., Gardner, G.H.F., 1998. Reducing 3-D acquisition footprint for 3-D DMO and 3-D prestack migration. Geophysics 63, 1177–1183.

Chadwick, A., Williams, G., Delepine, N., Clochard, V., Labat, K., Sturton, S., Buddensiek, M.L., Dillen, M., Nickel, M., Lima, A.L., Arts, R., Neele, F., Rossi, G., 2010. Quantitative analysis of time-lapse seismic monitoring data at the Sleipner CO_2 storage operation. Leading Edge 29, 170–177.

Cosma, C., Enescu, N., 2001. Characterization of fractured rock in the vicinity of tunnels by the swept impact seismic technique. International Journal of Rock Mechanics and Mining Sciences 38, 815–821.

Eiken, O., Brevik, I., Arts, R., Lindeberg, E., Fagervik, K., 2000. Seismic monitoring of CO_2 injected into a marine aquifer. SEG Calgary 2000 International Conference and 70th Annual Meeting, Calgary, Paper RC-.2.

Förster, A., Norden, B., Zinck-Jørgensen, K., Frykman, P., Kulenkampff, J., Spangenberg, E., Erzinger, J., Zimmer, M., Kopp, J., Borm, G., Juhlin, C., Cosma, C., Hurter, S., 2006. Baseline characterization of the CO_2SINK geological storage site at Ketzin, Germany. Environmental Geosciences 13, 145–161.

Ivanova, A., Kashubin, A., Juhojuntti, N., Kummerow, J., Henninges, J., Juhlin, C., Lüth, S., Ivandic, M., 2012. Monitoring and volumetric estimation of injected CO2 using 4D seismic, petrophysical data, core measurements and well logging: a case study at Ketzin, Germany. Geophysical Prospecting. http://dx.doi.org/10.1111/j.1365-2478.2012.01045.x.

Juhlin, C., Cosma, C., Förster, A., Giese, R., Juhojuntti, N., Kazemeini, H., Norden, B., Zinck-Jørgensen, K., 2006. Baseline 3D seismic imaging for the CO_2SINK project in the Ketzin area, Germany. Proceedings 8th Greenhouse Gas Technology Conference, Trondheim, Norway. CD-ROM.

Juhlin, C., Giese, R., Zinck-Jørgensen, K., Cosma, C., Kazemeini, H., Juhojuntti, N., Lüth, S., Norden, B., Förster, A., 2007. 3D baseline seismics at Ketzin, Germany: the CO_2SINK project. Geophysics 72, B121–B132.

Kazemeini, S.H., Juhlin, C., Fomel, S., 2010. Monitoring CO_2 response on surface seismic data; a rock physics and seismic modeling feasibility study at the CO_2 sequestration site, Ketzin, Germany. Journal of Applied Geophysics 71 (4), 109–124.

Kiessling, D., Schmidt-Hattenberger, C., Schuett, H., Schilling, F., Krueger, K., Schoebel, B., Danckwardt, E., Kummerow, J., the CO_2SINK Group, 2010. Geoelectrical methods for monitoring geological CO_2 storage: first results from cross-hole and surface-downhole measurements from the CO_2SINK test site at Ketzin (Germany). International Journal of Greenhouse Gas Control 4, 816–826.

Park, C.B., Miller, R.D., Steeples, D.W., Black, R.A., 1996. Swept impact seismic technique (SIST). Geophysics 61, 1789–1803.

Prevedel, B., Wohlgemuth, L., Henninges, Krüger, K., Norden, B., Förster, A., 2008. The CO_2SINK boreholes for geological storage testing. Scientific Drilling 6, 32–37.

Qin, F., Wang, B., Zhang, P., Audebert, F., 2005. Kirchhoff preSDM interactive dip-gather stacking and dip illumination panel generation. 75th Annual International Meeting, Soc. of Expl. Geophys. , pp. 1882–1885.
Rickett, J.E., Lumley, D.E., 2001. Cross-equalization data processing for time-lapse seismic reservoir monitoring: a case study 556 from the Gulf of Mexico. Geophysics 66, 1015–1025.
Robinson, E.A., Treitel, S., 1980. Geophysical Signal Analysis. Prentice-Hall. 466 p. Reprint, SEG, 2000.
Ross, C.P., Cunningham, G.B., Weber, D.P., 1996. Inside the cross equalization black box. The Leading Edge 15, 1233–1240.
Schmelzbach, C., Horstmeyer, H., Juhlin, C., 2007. Shallow 3D seismic-reflection imaging of fracture zones in crystalline rock. Geophysics 72, B149–B160.
Tang, Y., 2007. Selective stacking in the reflection-angle and azimuth domain. 77th Annual International Meeting, Soc. of Expl. Geophys. , pp. 2320–2324.
Yilmaz, O., 2001. Seismic Data Analysis. Society of Exploration Geophysicists.
Yordkayhun, S., Ivanova, A., Giese, R., Juhlin, C., Cosma, C., 2009. Comparison of surface seismic sources at the CO_2SINK site, Ketzin, Germany. Geophysical Prospecting 57, 125–139.

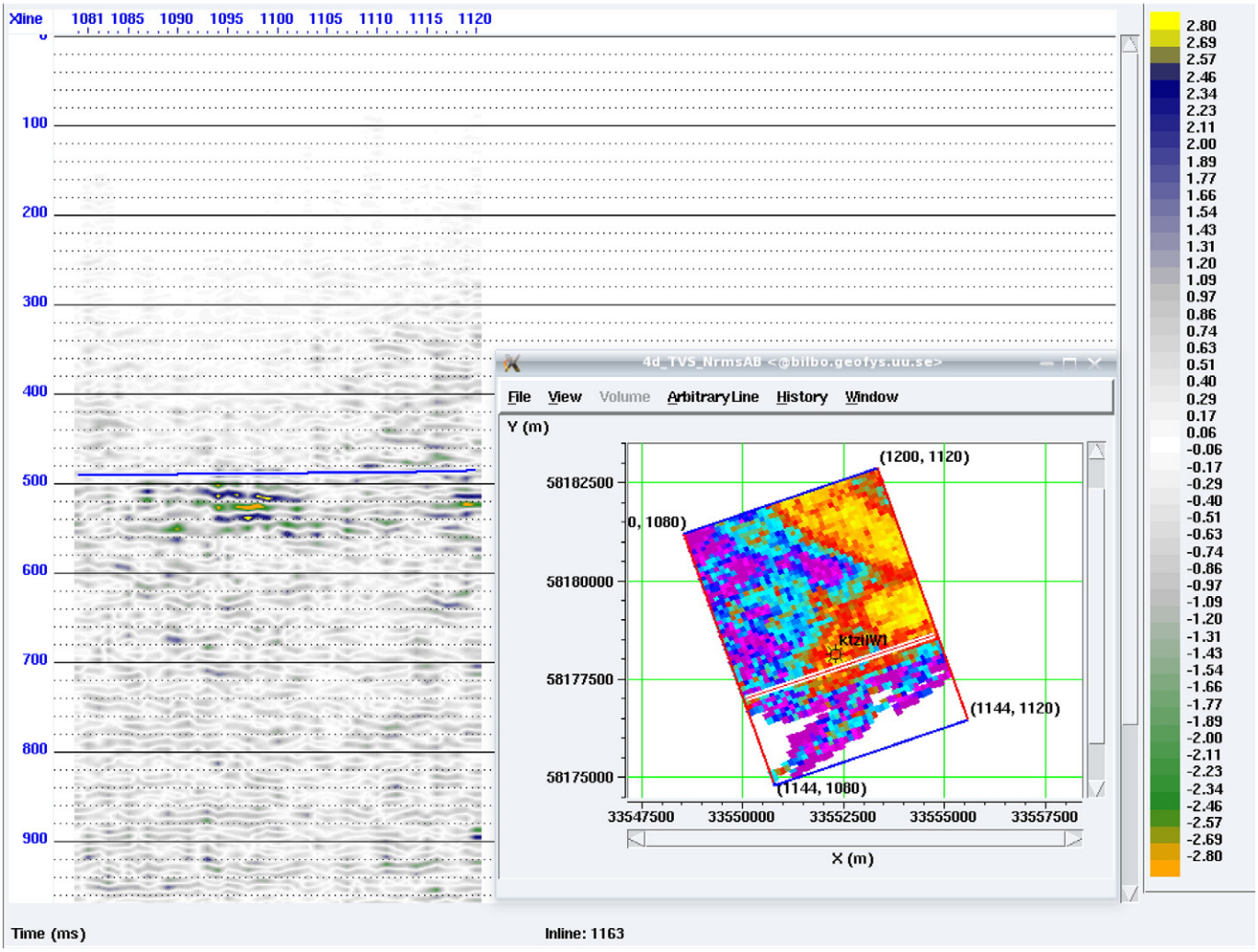

Fig. 13. Time-lapse processing results for the a) 1st repeat and b) 2nd repeat data sets along inlines 1163 and 1165, respectively. Colors highlight the difference between cross-calibrated volumes. The reflector K2 is shown as a blue line.

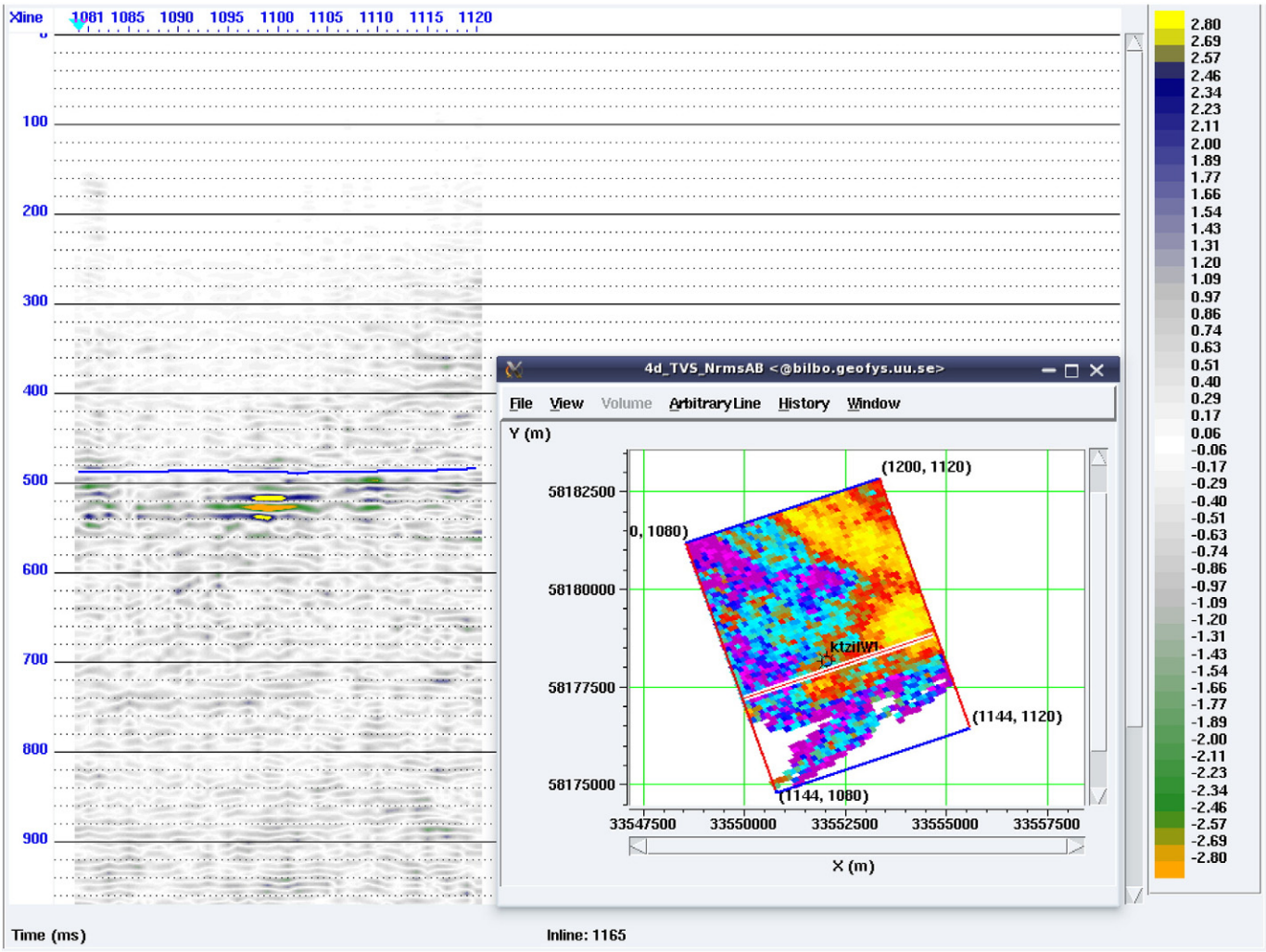

Fig. 13b (*continued*).

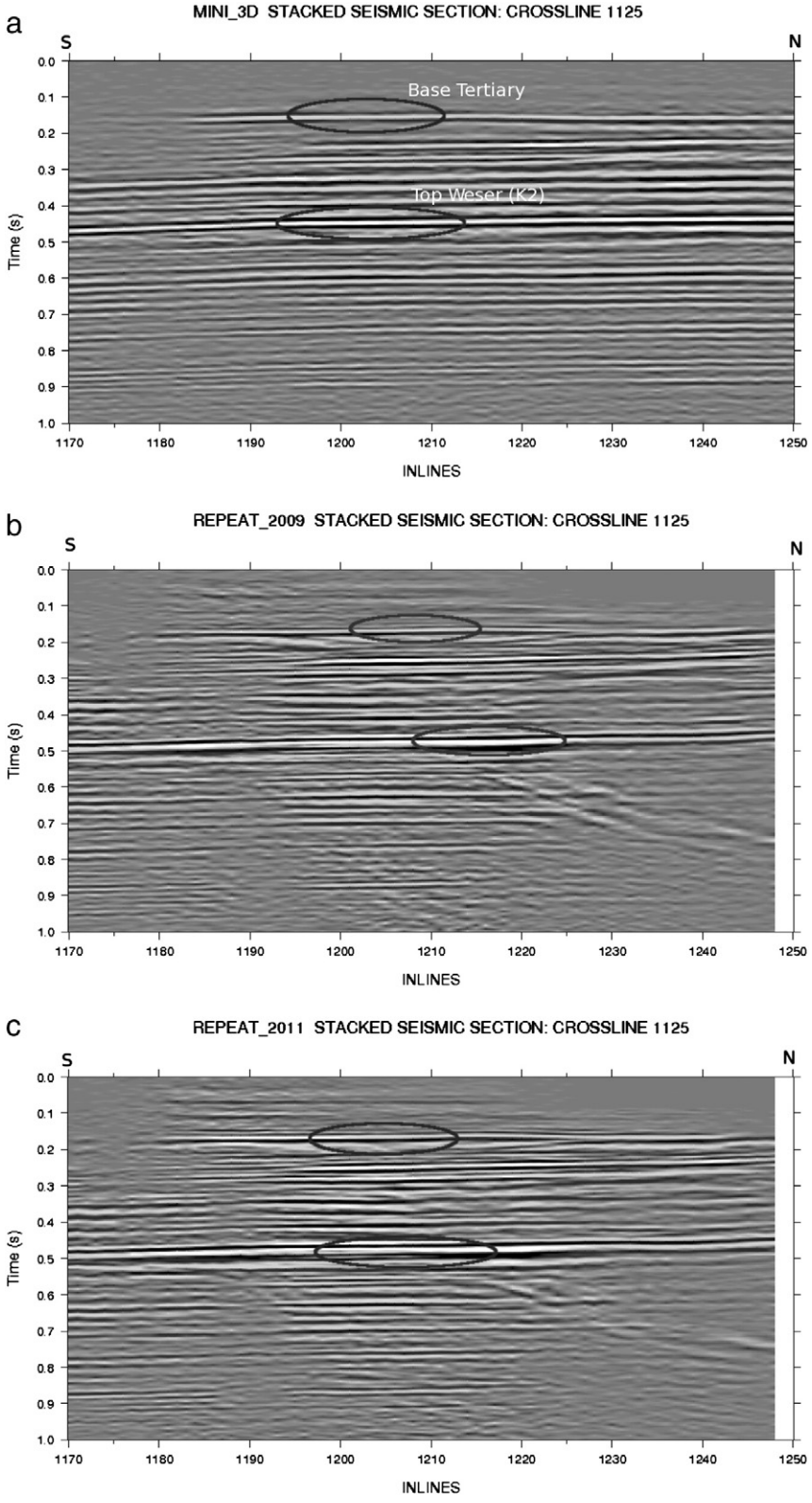

Fig. 14. Comparison of the stacked seismic sections from the three surveys: a) mini-3D, b) 1st repeat and c) 2nd repeat. The near Base Tertiary and Top Weser Formation (K2) are clearly identified.

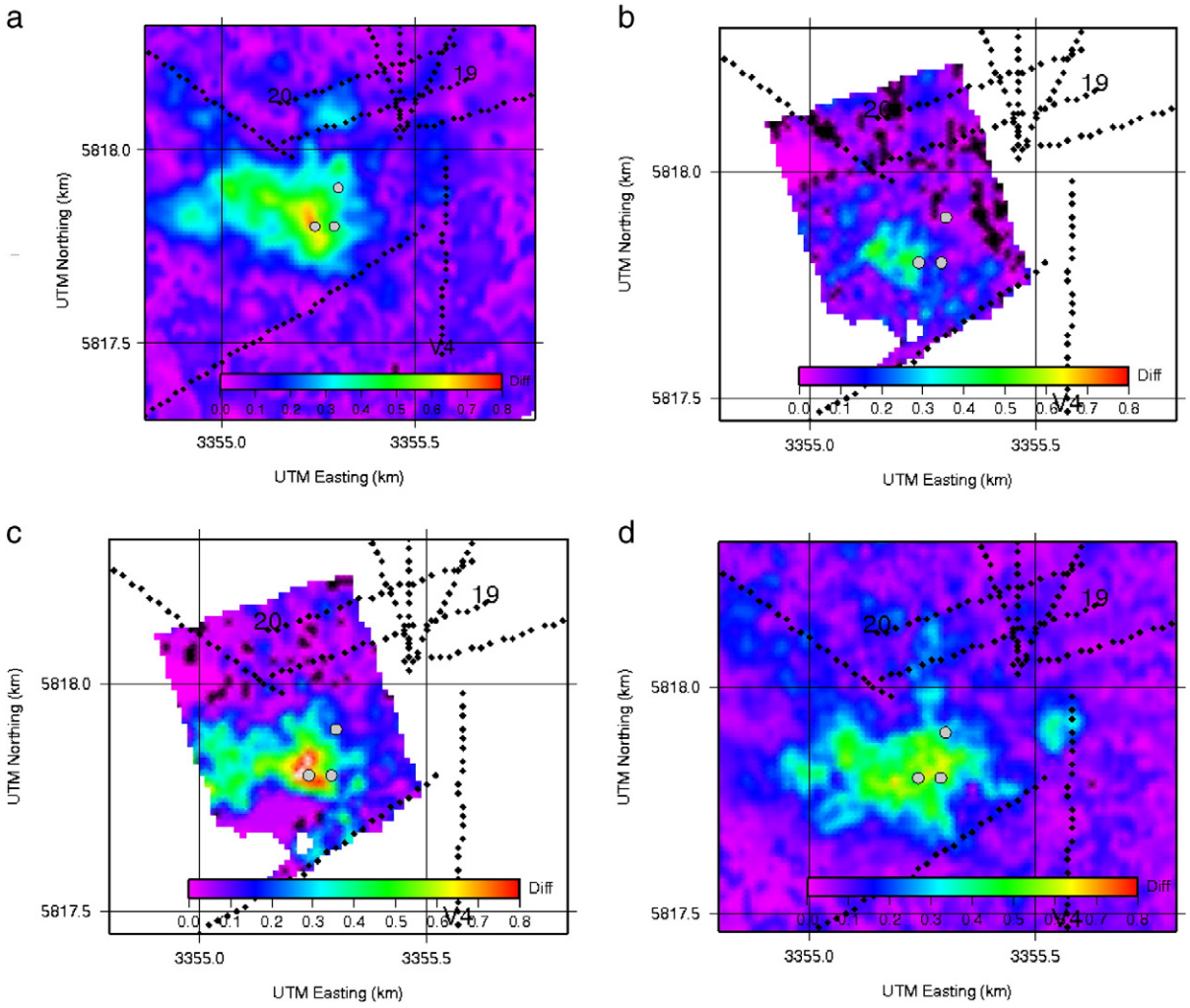

Fig. 15. Amplitude difference horizon at the reservoir level for the a) mini-3D, b) 1st sparse 3D repeat survey, c) 2nd sparse 3D repeat survey, and d) unmigrated mini-3D.